Dynamic Behavior of Water within a Polymer Electrolyte Fuel Cell Membrane at Low Hydration Levels

Adam M. Pivovar*,† and Bryan S. Pivovar‡

NIST Center for Neutron Research, National Institute of Standards and Technology, Gaithersburg, Maryland 20089, and Materials Science and Technology Division, Los Alamos National Laboratory, Los Alamos, New Mexico 87545

Received: September 2, 2004; In Final Form: October 21, 2004

Protonic conduction across the membrane of a polymer electrolyte fuel cell is intimately related to the dynamic behavior of water present within the membrane. To further the understanding of water dynamics in these materials, quasielastic neutron scattering (QENS) has been used to investigate the picosecond dynamic behavior of water within a perfluorosulfonated ionomer (PFSI) membrane under increasing hydration levels from dry to saturation. Evaluation of the elastic incoherent structure factor (EISF) reveals an increase in the characteristic length-scale of confinement as the number of water molecules in the membrane increases, tending to an asymptotic value at saturation. The fraction of elastic incoherent scattering observed at high Q over all hydration levels is well fit by a simple model that assumes a single, nondiffusing hydronium ion per membrane sulfonic acid site. The quasielastic component of the fitted data indicates confined dynamic behavior for scattering vectors less than 0.7 $Å^{-1}$. As such, the dynamic behavior was interpreted using continuous diffusion confined within a sphere at $Q < 0.7$ $Å^{-1}$ and random unconstrained jump diffusion at $Q > 0.7$ $Å^{-1}$. As the number of water molecules in the membrane increases, the characteristic residence times obtained from both models is reduced. The increased dynamical frequency is further reflected in the diffusion coefficients predicted by both models. Between low hydration (2 H_2O/SO_3H) and saturation (16 H_2O/SO_3H), the continuous spherical diffusion coefficient changes from 0.46 ± 0.12 to 1.04 ± 0.12 (10^{-5} cm^2/s) and jump diffusion indicates an increase from 1.21 ± 0.03 to 2.14 ± 0.08 (10^{-5} cm^2/s). Overall, the dynamic behavior of water has been quantified over different length scale regimes, the results of which may be rationalized on the basis of the formation of water clusters in the hydrophilic domain that expand toward an asymptotic upper limit with increased hydration.

Introduction

Realizing the benefits of hydrogen based energy systems requires the development of a diverse array of materials with properties that positively contribute to overall energy production including lower costs, higher efficiency, and reduced greenhouse gas emission.[1,2] Polymer electrolyte fuel cells (PEFCs) are one type of energy system that promises to exceed current energy conversion techniques. In PEFCs, protons and electrons are produced by catalytic conversion of a fuel, typically hydrogen, on the anode side of the fuel cell. A polymer electrolyte membrane (PEM) possesses covalently linked acidic functionalities that permit protons to pass directly to the cathode, while forcing the electrons through an external load that can be used as a source of electricity. Because the electronic power output of the cell is directly proportional to the transport of protons across the PEM, membranes with high proton conductivities are required before the full utility of PEFCs can be realized.

Typically, to attain the level of protonic conductivity needed for a functionally useful PEFC, PEMs are swelled with water through humidification or direct contact with an aqueous environment.[3,4] In the absence of water, PEM resistance to protonic conduction is very large, yielding pragmatically useless currents.[3] The water molecules modify both the structural conduit and dynamic behavior of the molecules involved in protonic conduction, resulting in improved ion transport with increased swelling.[4] However, increased hydration levels may hinder fuel cell operation by enhancing flooding at the cathode. As such, a detailed description of water's role in altering the structure and dynamics of a PEM is critically important for understanding the mechanism of protonic conductivity and advancing the development of new materials for use in PEFCs.

Perfluorosulfonated ionomer (PFSI) membranes have become popular PEM materials for PEFC applications, the most common of which goes by the trade name Nafion. [Trade names are mentioned to provide complete identification of experimental conditions and such identification is not intended as an endorsement by NIST or LANL.] These PFSI ionomers consist of hydrophilic sulfonic acid terminated side groups tethered by a fluoroether linkage to a hydrophobic poly(tetrafluoroethylene) backbone. On a macroscopic level, PFSI membranes are useful because they are highly durable and can be processed in a relatively facile manner. Microscopically, water selectively incorporated into the hydrophilic domain facilitates protonic conductivity by solvating the sulfonic acid moieties, swelling the hydrophilic pores and forming a continuous conduction pathway across the membrane.[3] Although there is disagreement regarding the exact structural model of hydrated Nafion membranes, many NMR,[5,6] small-angle scattering,[7−13] IR,[14−17] microscopy,[18,19] and molecular dynamics[20,21] studies have

* Corresponding author. E-mail: adam.pivovar@nist.gov.
† National Institute of Standards and Technology.
‡ Los Alamos National Laboratory.

10.1021/jp046029x CCC: $30.25
Published on Web 12/08/2004

confirmed water clustering within hydrophilic domains that are nanophase separated from the hydrophobic backbone.

In addition to enhancing phase segregation and providing a conduit for conduction, the dynamic behavior of the water molecules is also intimately correlated with the magnitude and mechanism of protonic conductivity, reactant permeability and electro-osmotic drag in PFSI membranes.[22−25] Yet, although there have been extensive investigations regarding the structural properties of PFSI membranes as a function of hydration, fewer studies regarding the dynamic behavior of water molecules within swelled membranes have been performed. To date, the main technique used to directly measure the self-diffusion behavior of membrane water has been pulsed field gradient nuclear magnetic resonance spectroscopy.[5,22,26−28] However, because the PFG-NMR technique probes dynamic behavior on microsecond time-scales, it has poor sensitivity to localized dynamic events on the molecular scale.[25,29] Another technique highly suitable for measuring the dynamics of water within PFSI membranes is quasielastic neutron scattering (QENS). Though unable to provide the same mesoscopic scale information as NMR, QENS is much more sensitive to the local diffusive environment because it probes dynamic events on the picosecond time scale and molecular length scale.[25]

The utility of QENS for investigating the diffusion of water within a PFSI membrane has already been demonstrated by a previous study on a completely saturated membrane.[30,31] During the operation of a PEFC, however, the membrane will likely experience a range of hydration levels between the dry and saturated states. This is particularly true in the course of fuel cell start up where water produced at the cathode is used to swell the membrane until the desired steady state behavior is achieved and for high-temperature low-pressure operation where complete humidification is difficult to achieve. To gain a deeper understanding of the interdependence between the dynamic behavior of water molecules and protonic conductivity within PEMs over the low swelling range of water content, we have performed QENS measurements on a PFSI membrane under increasing hydration levels, from completely dry to near saturation

Experimental Section

Materials and General Procedures. The PEM material, Nafion 117, was purchased from Ion Power (Bear, DE). Nafion 117 has an ionic equivalent molecular weight of 1100 g/(mol of sulfonic acid group) and a dry thickness ≈178 μm. The experimental sample consisted of a single 5 cm by 10 cm rectangular strip. To remove impurities, the sample was placed in 500 mL of 1 mol/L sulfuric acid solution at 100 °C for 1 h. After the acid treatment, residual acid was removed from the membrane by placing it in 1 L of boiling, deionized water for approximately 30 min, after which it was transferred into 1 L of room temperature deionized water until cool. The membrane was repeatedly rinsed with deionized water, patted dry, rolled, and placed into an open cylindrical aluminum sample holder (length = 5 cm; diameter = 1.25 cm). This procedure resulted in an annular sample of approximately 450 μm thickness. The sample was dried in vacuo at 100 °C for 16 h, and the sample cell sealed from the atmosphere. The mass of the completely dried sample was 1.68 g.

Starting from a completely dry membrane, the sample was hydrated by adding water to the sample cell in amounts equal to stoichiometric equivalents of sulfonate groups in the membrane (1 mol of water/mole of SO_3^- is equal to 27.5 mg of water for the sample). After the water was rapidly added and the cell sealed, the sample cell was placed in an oven at 70 °C for 3 h to uniformly equilibrate the water within the membrane. The sample was allowed to come to room temperature for at least 1 h before collecting a QENS spectrum. Several hydration levels (λ = moles of water/moles of sulfonic acid sites) between dry ($\lambda = 0$) to near saturation ($\lambda = 16$) were analyzed. Assuming a 200 μm thick annular sample of pure liquid water scatters 10% of the incident neutrons, the relative hydrogen density of our sample at saturation results in less than 5% scattering of the incident neutron beam, as such, the contribution of secondary scattering from our samples over all hydration levels is negligible.

Theory. In a neutron scattering experiment, both momentum and energy transfer are measured. The momentum transferred to the sample is described by the scattering vector, Q, defined by the final minus the incident neutron wavevectors (i.e., $Q = k - k_0$). Energy transfer is defined by the final minus the incident neutron energy using the equation $\hbar\omega = E - E_0$. Overall, the total neutron scattering measured in a typical experiment contains contributions from both coherently and incoherently scattered neutrons.

$$S_{\text{total}}(Q,\omega) = S_{\text{coh}}(Q,\omega) + S_{\text{inc}}(Q,\omega) \tag{1}$$

where the coherent component, $S_{\text{coh}}(Q,\omega)$, due to constructive interference between neutrons scattered from different scattering sites reflects of structural features within the sample. On the other hand, the incoherent component represents scattering from the interaction of a single neutron with a single scattering site.

Quasielastic Neutron Scattering. In a typical QENS experiment, a sample is irradiated with a monochromatic beam of neutrons with well-defined energy. These incident neutrons are scattered by exchanging momentum and energy with the sample. Quasielastic scattering is centered at zero energy transfer and consists of a relatively broad component arising from diffusive or relaxational motions. Often there is also a narrow elastic component also centered at zero energy transfer arising from confinement or coherent scattering with a width determined solely by the instrumental resolution. The Q dependence of the quasielastic width and the relative intensities of the elastic and quasielastic components give information on the geometry of the motions involved.

An important feature of neutron scattering is the extremely large, and primarily incoherent, scattering cross section[32] of hydrogen (82.02 barns) as compared to any other atomic species, especially carbon (5.551), fluorine (4.018), sulfur (1.026), and oxygen (4.232) (the atomic components of a PFSI) and deuterium (7.64). As such, the vast majority of quasielastic scattering, as distinguished from elastic scattering, from water swelled fluoro-ionomer membranes is attributable to the hydrogen atoms of H_2O. This fundamental aspect of neutron scattering, in combination with the atomic composition of the fluoro-ionomer, permits the water dynamics within a PFSI membrane to be ascertained directly from the scattering data.

The QENS data were collected at 295 K with the Fermi Chopper spectrometer (FCS) located on neutron guide NG6 at the National Institute of Standards and Technology Center for Neutron Research.[33] The complete two-dimensional time-of-flight scattering profile ($S(Q,\omega)$) was collected in the Q range from 0.4 to 2.0 Å^{-1}. The spectra were obtained with an incident wavelength of 6 Å, yielding an instrument resolution between 55 and 70 μeV and a total energy range of −2.0 to +1.0 meV. The time-scale resolution of this configuration, following the method of Doster et al., corresponds to approximately 16 ps.[34] The quasielastic component of the spectra, therefore, includes

water motions faster than a few tens of picoseconds, typical of random diffusion of water in porous media at room temperature. Because the QENS spectra contain information regarding the exchange energy and momentum transferred by neutrons to the hydrogen atoms of the sample, it is possible to extract information on the form, amplitude, and time dependence of the molecular motions using simple physical models.

Data Analysis and Fitting. The collected QENS time-of-flight spectra were analyzed between −0.75 and +0.75 meV using the *xtreat* program available at the NCNR.[35] Energy exchange values >0.75 meV contain no quasielastic scattering and, hence, were excluded from our analysis. The experimental data contained neutrons scattered both elastically and quasielastically, corresponding to immobile and dynamic hydrogen atoms, respectively. By assuming this physical picture, we were able to account for the different features of the experimental data using the following function

$$S_{\mathrm{exp}}(Q,\omega) = I(Q)(x\cdot R(\omega) + (1-x)R(\omega) \otimes L(\omega)) + B_0 \quad (2)$$

$S_{\mathrm{exp}}(Q,\omega)$ is the experimentally measured spectrum, $I(Q)$ the scaled intensity at a given Q, $R(\omega)$ the resolution function of the instrument, $L(\omega)$ a Lorentzian distribution, and B_0 a flat background. The value x in eq 2 corresponds to the quantity referred to as the elastic incoherent structure factor (EISF, the fraction of elastically scattered neutrons), which provides information regarding the relative length scale of the hydrogen dynamics. The quantity $x\cdot R(\omega)$ is the contribution from the elastically scattered neutrons and $(1-x)R(\omega) \otimes L(\omega)$ corresponds to the contribution from the neutrons quasielastically scattered from diffusing hydrogen atoms convoluted with the instrument resolution.

The fwhm of the resolution function ($R(\omega)$) was obtained by collecting an experimental spectrum of the $\lambda = 16$ sample at 100 K and fitting the spectrum with a Gaussian function for each Q. At 100 K the water molecules are frozen and elastically scattered neutrons dominate the spectrum. The Q dependence was fit to a smooth quadratic equation yielding a resolution function of fwhm $(Q) = 5.72 \times 10^{-2} + 4.66 \times 10^{-3}Q + 5.83 \times 10^{-4}Q^2$ (meV). Though the resolution of some neutron scattering instruments is complex and not amenable to approximation by a simple Gaussian line shape, the FCS instrumental resolution is extremely well fit by this procedure. By fixing the instrumental resolution, the remaining parameters extracted from the experimental data were reduced to x and $L(\omega)$.

Many self-diffusion models have been used to interpret QENS obtained from molecules within porous matrixes.[36] In the present investigation, the QENS data have been analyzed with both diffusion in a sphere and jump diffusion models based on fitting the quasielastically scattered neutrons with a single Lorentzian function ($L(\omega)$ in eq 2). Although using these models to interpret QENS data fit by a single Lorentzian function often gives simplified approximations of real experimental systems, the models are useful for extracting consistent parametrized information regarding time-scale, length scale and self-diffusion coefficients from the neutron data. Furthermore, because of the relatively short time scale measured and broad energy resolution of the FCS instrument, attempts to use more rigorous fitting protocols, i.e., stretched exponential or multiple Lorentzian, gave poor fits that were not amenable to interpretation.

The continuous diffusion within a sphere model was developed by Volino and Dianoux[30] and has previously been employed for interpreting the diffusion behavior of water in a completely hydrated Nafion membrane.[31] The scattering law for this model is

$$S_{\mathrm{inc}}(Q,\omega) = A_0^0(Q)\,\delta(\omega) + \frac{1}{\pi}\sum_{\{n,l\}\neq\{0,0\}}^{\infty}(2l+1)A_n^l(Q)\frac{(x_n^l)^2 D_{\mathrm{local}}/R^2}{[(x_n^l)^2 D_{\mathrm{local}}/R^2]^2 + \omega^2} \quad (3)$$

where

$$A_0^0(Q) = \left(\frac{3j_1(QR)}{QR}\right)^2 \quad \text{with} \quad j_1(QR) = \frac{\sin(QR)}{(QR)^2} - \frac{\cos(QR)}{QR} \quad (4)$$

$$A_n^l(Q) = \frac{6(x_n^l)^2}{(x_n^l)^2 - l(l+1)}\left(\frac{QRj_{l+1}(QR) - lj_l(QR)}{(QR)^2 - (x_n^l)^2}\right)^2 \quad (5)$$

Here, R is the characteristic radius of the sphere within which the dynamics occur and j_n is the nth spherical Bessel function. The quantity x_n^l is determined by the boundary conditions assuming an impermeable spherical surface; Volino and Dianoux have tabulated the first 99 values of x_n^l.[30] In the spherical diffusion model, confinement results in a constant value of the half-width at half-maximum (HWHM) of the quasielastic contribution at low Q. At high Q, the HWHM tends to pure Fickian diffusion with DQ^2 dependence.

The first term of eq 4, $A_0^0(Q)$, represents the elastic contribution to the overall scattering. The elastic component is added to the second term, which is the infinite sum of broad Lorentzian line shapes representing the quasielastic component of the scattering. As such, the spatial distribution of the diffusing hydrogen atoms can be determined from the experimental data fit by eq 3 and the spherical diffusion model using the following correlation of the EISF:

$$x = \mathrm{EISF} = f_{\mathrm{ND}} + (1 - f_{\mathrm{ND}})\left(\frac{3j_1(QR)}{QR}\right)^2 \quad (6)$$

Where f_{ND} accounts for the number of hydrogen atoms that are not diffusing within the time window of the experiment (i.e., immobile).

Information regarding the diffusive motions of water molecules can be ascertained from the Q dependence of the HWHM (Γ) of the quasielastic component of the neutron scattering data. In this study, the dynamic behavior is modeled by the unconstrained random jump diffusion with a Gaussian distribution of jump lengths developed by Hall and Ross.[37] This predicts quasielastic broadening given by

$$\Gamma(Q) = \frac{1}{\tau}\left[1 - \exp\left(\frac{-Q^2\langle r^2\rangle}{6}\right)\right] \quad (7)$$

where τ is the residence time between jumps and $\langle r^2\rangle$ is the mean square jump length, which is related to the characteristic jump length r_0 by $\langle r^2\rangle = 3r_0^2$. The jump diffusion model follows a linear Fickian diffusion ($\Gamma(Q) = DQ^2$) at low Q and tends at high Q to an asymptotic value of $\Gamma(Q) = 2/\tau$. From the

parameters extracted from a fit using eq 8, the self-diffusion coefficient can be calculated using

$$D_{\text{jump}} = \frac{\langle r^2 \rangle}{6\tau} \tag{8}$$

Error Estimation. The values and uncertainty of the diffusion model parameters obtained from the fitting protocol were estimated using a Monte Carlo method that extracted an overall average value from the fit parameters of many (>10 000) synthetic data sets.[38] Starting from the value and statistical error of the parameters obtained by fitting the data with eq 3, a single synthetic data set represents an array of data points calculated by a random, error weighted Gaussian probability about the original value. The standard deviation of the best-fit values was determined from standard least-squares analysis of the extracted best-fit values for each synthetic data set. The suitability of this method for interpreting quasielastic neutron scattering data has been demonstrated previously[39] and is more robust than a standard least-squares method of error estimation here because of the nonlinear correlation between the model parameters and data.

Results and Discussion

QENS spectra on a single PFSI membrane were collected over a range of hydration conditions, beginning with a completely dried membrane. The hydration was increased between $\lambda = 1$ and 16 by adding molar equivalents of water to the sample container and allowing equilibration with the membrane. Owing to the large incoherent neutron scattering cross section of hydrogen relative to the atomic makeup of the polymer membrane, the incoherent, quasielastic neutron scattering is primarily due to scattering from the hydrogen atoms. This was also confirmed by observing an exceedingly small intensity of incoherently scattered neutrons collected on a membrane swelled with D_2O. Hence, data interpretation was simplified by ignoring the negligible scattering intensity contributed to the quasielastic signal from the polymeric backbone and assuming that the entirety of measured quasielastic scattering was directly attributable to water dynamics.

Experimental data from a representative QENS spectrum collected on the PFSI membrane at $\lambda = 6$ are depicted in Figure 1 at Q values of 0.592 and 1.70 Å^{-1}. The data are provided only for the -0.4 to $+0.4$ meV energy range to facilitate depiction of the quasielastic component of the total scattering. Included with the experimental data are the best overall fit and the individual contributions from the Gaussian resolution, Lorentzian line shape, and flat background according to the data analysis scheme (eq 2). As observed by the residual difference, the model provides a good fit to the experimental data. At low hydration levels ($\lambda < 2$) where few hydrogen atoms are present in the system, the goodness-of-fit is degraded on account of the low intensity of incoherently scattered neutrons yielding poor signal-to-noise ratios in the recorded data. As such, fitting the QENS spectrum of the dry membrane was not possible and statistical errors from the analysis at $\lambda = 1$ tends to be relatively large.

Figure 2 contains plots comparing the integrated intensity extracted from the area under the curve of the elastic component of the fitting procedure on hydrogenated and deuterium exchanged membranes in dry ($\lambda = 0$) and saturated ($\lambda = 16$) states. The integrated intensity of the $\lambda = 1$ sample containing hydrogenated water is also given. The intensity measured from deuterium-exchanged samples contains neutrons coherently scattered from the structural arrangement of the backbone of the membrane polymer and neutrons incoherently scattered from deuterium. For the hydrogen containing samples, the total elastic scattering contains contributions from both neutrons incoherently scattered by hydrogen atoms and the coherent backbone scattering. As is apparent from the deuterium-exchanged measurements, the elastic intensity has a strong Q dependence with a large peak apparent in the 0.9−1.5 Å^{-1} range. This feature is primarily due to coherent scattering from the polymer backbone, whereas outside the peak, the elastic intensity includes incoherent scattering from the deuterium atoms. Although the backbone scattering peak is also apparent in the hydrogenated

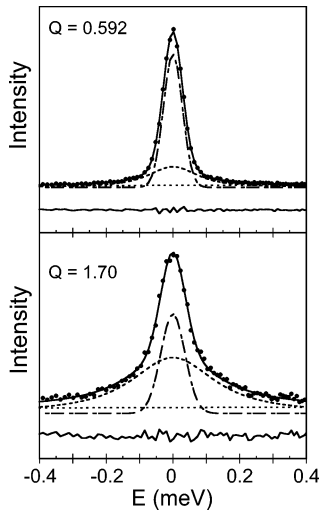

Figure 1. Plots of the experimental quasi-elastic neutron scattering data collected on a perfluorosulfonated ionomer membrane hydrated with 6 water molecules per sulfonic acid functionality ($\lambda = 6$) at $Q = 0.592$ Å^{-1} and $Q = 1.70$ Å^{-1}. The closed circles (●) represent the experimental data and the solid line through them corresponds to the overall model fit (eq 3). The overall model fit is composed of the instrument resolution function (dashed line, - - -), a Lorentzian line (short−long dashed, − —), and a flat background (dotted line, ···). The goodness-of-fit is indicated by the residual difference between the experimental data and the overall fit (bottom solid line).

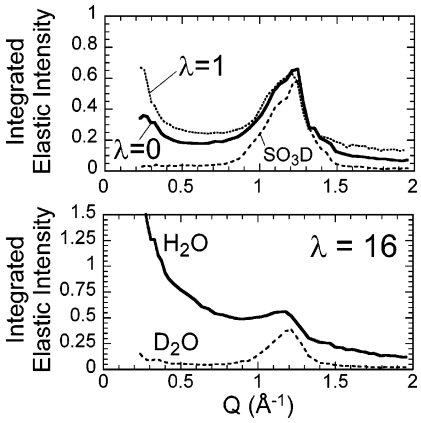

Figure 2. Plots comparing the integrated elastic intensity of a perfluorosulfonated ionomer membrane under hydrogenated and deuterium exchanged conditions at dry and low hydration ($\lambda = 0$, 1; top) and saturated swelling ($\lambda = 16$; bottom). The top panel gives the integrated elastic intensity over the measured Q range for a hydrogenated sample at $\lambda = 1$ (···) and $\lambda = 0$ (—) in addition to the deuterium exchanged sample at hydration level equivalent to $\lambda = 0$, depicted as SO_3D (- - -). The bottom panel compares the integrated elastic intensity at the highest hydration condition measured, $\lambda = 16$, for the water (H_2O, solid line) and deuterium oxide (D_2O, dashed line) swelled samples.

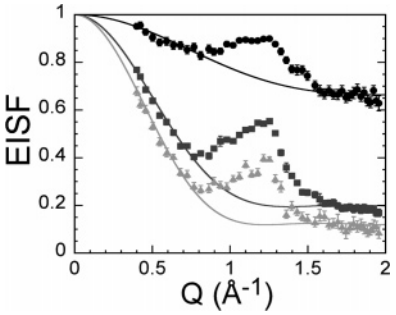

Figure 3. Elastic incoherent structure factor (EISF) as a function of Q at different levels of water swelling. The experimental data points were obtained from the fit of the QENS spectra at $\lambda = 2$ (●), 6 (■), and 16 (▲), and the solid lines correspond to the best fit obtained with the theoretical diffusion in a sphere model.

samples, the contribution of neutrons incoherently scattered from water molecules is greater because the relative scattering cross-section of hydrogen is approximately an order of magnitude larger than deuterium.

Comparison between the intensity of hydrogen and deuterium samples allows one to estimate the relative contribution of the coherent backbone scattering to the overall elastic scattering. Clearly, the relative magnitude of the deuterium-exchanged samples to the hydrogenated samples are, as expected, strongest in the Q range containing the structural peak, with the deuterium-exchanged samples amounting to 87% and 74% of the total elastic intensity at $Q = 1.215$ Å^{-1} for the dry and saturated samples, respectively. Outside the Q range of the strong coherent peak the relative scattering intensity of the hydrogenated sample is amplified. For example, the relative intensity of the deuterium-exchanged sample to the hydrogenated sample at $Q = 0.592$ Å^{-1} is only 16% for the dry sample and 6% for the wet sample and at $Q = 1.70$ Å^{-1} is 26% for the dry sample and 8% for the wet sample. Similar analysis of the data at $\lambda = 1$ (comparing against the dry, deuterium exchanged sample) indicates that the deuterium exchanged sample scattering has approximately 11% of the intensity at 0.592 Å^{-1}, 90.5% at 1.215 Å^{-1}, and 10% at 1.70 Å^{-1} of the hydrogenated sample. A "worst case" estimate of the contribution from backbone coherent scattering to the total elastic intensity in the Q-range outside of the structural peak would therefore be about 10−11% at low λ and 6−8% at high λ. This "worst case" estimate, however, assumes no contribution to the elastic scattering intensity from neutrons incoherently scattered by deuterium atoms in the deuterium-exchanged samples. Accounting for these incoherently scattered neutrons adjusts the estimated contribution from the backbone to approximately 6−8% at $\lambda = 1$ and 2−3% at $\lambda = 16$.

From the Gaussian resolution and Lorentzian components of the overall fit, it is possible to extract the contribution from elastic and quasielastic scattering, respectively. The fractional contribution of elastic scattering to the total incoherent scattering intensity, a quantity commonly used to analyze dynamic length scales, is referred to as the elastic incoherent structure factor (EISF).[40] The EISFs extracted from fits of the QENS spectra at λ of 2, 6, and 16 are provided as a function of scattering vector in Figure 3 along with the best fit theoretical EISF for continuous diffusion in a sphere (eq 6).[30] Though it is unlikely that the dynamical behavior of water molecules within the amorphous PFSI membrane occurs in a rigorously spherical spatial envelope, the model does provide a means of extracting quantitative, sample-averaged length-scale information from the scattering data. Additionally, even though at high Q (atomic length scales) diffusion follows a noncontinuous mechanism, the model accounts for this contribution to the EISF and is still able to provide information regarding the confinement length scale. The propriety of assuming spherical confinement is, however, supported by the models used to interpret membrane morphology in small angle scattering investigations performed on similar PFSI membranes at low swelling conditions.[11]

Comparison of the EISF value with increasing water loading in the membrane at all scattering vectors displays a reduced magnitude of the relative fraction of elastic to quasielastic scattering, revealing an increase in the overall proton dynamics as the number of water molecules within the hydrophilic domain increases. This reflects the fact that as the hydrophilic phase swells, water in the center of the pores becomes more bulklike, and restrictive interactions between the water and the polymer diminish. At each individual hydration level, the EISF trend with scattering vector indicates an overall decrease in incoherent elastic intensity with increasing Q. However, as indicated by the plots of integrated elastic intensity given in Figure 2, coherently scattered neutrons from structural arrangement of the polymeric backbone chains add intensity to the elastic scattering, resulting in a peak in the EISF over an approximate Q range of 0.85 to 1.5 Å^{-1}.[31] Comparison of the percent contribution of the coherent backbone scattering to the total elastic intensity outside of the structural peak indicates that the contribution accounts for an average of around 4% of the total scattering. Unfortunately, attempts to remove the coherent contribution to the EISF by subtracting a QENS spectrum collected on the membrane swelled with D_2O were unsuccessful and one should be aware of this slight overestimation in the elastic contribution to the values of the EISF.

To avoid complications arising from coherent elastic scattering, the theoretical fit of the experimental EISF data was limited to the Q regions with intensity primarily due to incoherent scattering (i.e., $Q = 0.4-0.85$ Å^{-1} and $1.5-2.0$ Å^{-1}). Apparent by fits of the data in Figure 3, the model is able to approximate the experimental data over the fitting range rather well. Though it should be pointed out that the experimental EISF values do not reach fully flat behavior as that obtained by the fit model at high Q, indicating that the actual dynamic behavior is more complex than that approximated by the simple model. Although ignoring the intermediate Q range may appear problematic, systematic error in application of the theoretical spherical diffusion model is reduced because the fit parameters are particularly sensitive to the slope at low Q and the value at high Q. The parameters extracted from the model, therefore, should not be appreciably distorted by limiting the Q range of the fitting protocol except by the slight overestimation based on the small contribution to the elastic intensity from coherent scattering from the polymer backbone.

The characteristic radii (R) and fractions of nondiffusing scattering sites (f_{ND}) obtained by fitting the experimentally obtained EISF with the continuous diffusion confined in a sphere model are listed in Table 1 and graphically depicted in Figures 4 and 5, respectively, over the entire hydration range. Error estimation was performed by fitting a number of synthetic data sets generated from the experimental EISF using the Monte Carlo method discussed in the Experimental Section. The Monte Carlo method proved to be a reliable means of fitting the EISF because it is responsive to the subtleties of the theoretical model and accounts for imprecision in the QENS data.

The radius of the confining spherical volume given in Figure 4 is characterized by two regions: (1) a low hydration region up to $\lambda \approx 7$ where the size of confinement expands linearly, and (2) an asymptotic behavior as the membrane approaches

TABLE 1: Spherical Radius of Confinement (R) and Fraction of Nondiffusing Scattering Sites (f_{ND}) Obtained from the Best Fit to the EISF of the Continuous Diffusion in a Sphere Model for All Measured Hydration Levels

λ	R (Å)	f_{ND}	f_{ND}^{theo} [a]
1	2.10 ± 0.22	0.852 ± 0.010	1.000
2	2.24 ± 0.08	0.664 ± 0.006	0.600
3	2.61 ± 0.04	0.449 ± 0.004	0.429
4	2.93 ± 0.03	0.308 ± 0.004	0.333
5	3.08 ± 0.03	0.241 ± 0.003	0.273
6	3.27 ± 0.02	0.195 ± 0.003	0.231
8	3.46 ± 0.04	0.169 ± 0.006	0.176
10	3.56 ± 0.04	0.153 ± 0.005	0.143
12	3.55 ± 0.04	0.126 ± 0.005	0.120
16	3.66 ± 0.03	0.119 ± 0.005	0.091

[a] $f_{ND}^{theo} = 3/(3 + 2(\lambda - 1))$.

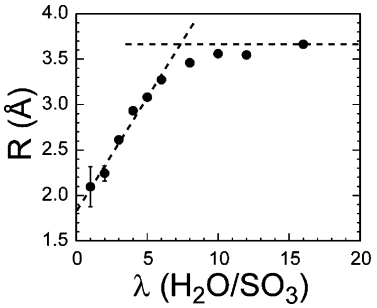

Figure 4. Values of the dynamical sphere radius (R) obtained from best fits of the theoretical EISF (eq 7) as a function of hydration. Dashed lines correspond to the slope over the low swelling regime and asymptotic value apparent over the highly swelled regime.

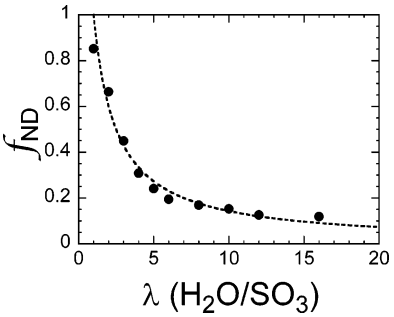

Figure 5. Experimentally determined (filled circles) and theoretically calculated (dashed line) fraction of nondiffusing hydrogen atoms (f_{ND}) plotted as a function of water swelling. The dashed line corresponds to the theoretical line obtained by assuming a single, nondiffusing hydronium ion (H_3O^+) for each sulfonic acid site in the membrane.

full water saturation. A simple linear fit to the low hydration radii yields $R(\lambda<7) = 1.83$ Å $+ 0.25(\lambda)$ Å, and at high swelling R(saturation) tends to 3.68 Å (dashed lines in Figure 3). The difference between R(saturation) of this study and that of a previous QENS investigation on a completely saturated PFSI membrane ($R = 4.25$ Å)[31] is likely the result of dissimilar membrane sulfonic acid density, membrane pretreatment, spectral Q range, and instrumental resolution.

Increase in R upon hydration of the membrane results from water clustering near the sulfonic acid sites of the membrane, expanding the size of the localized confinement provided by the hydrophobic phase. Over the hydration range between dry and approximately $\lambda = 7$, hydrophilic clusters are small enough that a majority of the water molecules experience interactions with the confining surface over the ~16 ps time scale of the experiment. Continued swelling causes water domains to grow and on average fewer of the molecules feel the confinement during the time scale probed by the measurement. Hence, utilizing the QENS data to determine structural confinement from dynamic behavior is limited by the time resolution of the instrument and a plateau is observed at high λ. Accounting for these fundamental properties of the QENS measurement technique allows one to rationalize the difference between the 16.5 Å structural radius of confinement measured by small angle scattering[9] and the dynamic spherical confinement radius between 2 and 3.7 Å of this study.

For a system where every particle is freely diffusing, the theoretical EISF predicted by the diffusion in a sphere model is expected to reach zero as a function of Q. This assumes that over very short length scales (i.e., large Q) all particles appear dynamic and no elastic scattering should occur. When there are nonmoving particles within the time window of the experiment, however, the EISF will trend to a finite value at high Q. This nonzero value represents the fraction of nondiffusing scattering sites present in the system. The fractions of nondiffusing hydrogen atoms as a function of water loading in the membrane obtained from fits of the EISF are plotted in Figure 5 along with a line representing the "theoretical" number of nondiffusing protons assuming a simplified model of one fixed hydronium ion per membrane sulfonic acid site. The theoretical nondiffusing model was constructed to test the results obtained with those of IR studies indicating a hydronium cation (H_3O^+) hydrogen bonded to a sulfonate (SO_3^-) at low membrane hydration levels.[41−43] The model also finds support in recent MD investigations, indicating that both the mean square displacement of the hydronium ion is significantly less than that of the neutral water molecules[20] and the hydronium ions remain adsorbed on the anionic site over time scales orders of magnitude longer than that probed by our QENS measurements.[21,44] Because the hydrogen atoms dominate the scattering, the model simply accounts for three fixed hydrogen atoms (corresponding to the hydronium ion) per sulfonate at each swelling condition using the relation

$$f_{ND}^{theo} = \frac{3}{3 + 2(\lambda - 1)}$$

Comparison between theoretical and experimental f_{ND} shows good agreement under all swelling conditions. Failure of the experimental value to reach unity at $\lambda = 1$ is likely due to an inhomogeneous distribution of water molecules in the membrane where some water molecules remain neutral and unbound. Overall, the physical picture of a single nondiffusing hydronium ion per anionic site is strongly supported by our data across all hydration levels. This result is somewhat unexpected because spectroscopic and theoretical investigations indicate formation of larger ionic species ($H_5O_2^+$, $H_9O_4^+$, etc.) should be expected as the hydration level increases.[4,25,41,43] Thus, it is possible that the behavior observed here may be the result of a distribution of nondiffusing ionic species, with a serendipitous coincidence between the fraction of fixed hydrogen atoms predicted by the simple model and the more complex dynamical behavior actually present in the system.

Information regarding the mechanism of water diffusion in the membrane is contained in the quasielastic component of the QENS spectrum. In our model, the quasielastic broadening at a given scattering vector is fit by a Lorentzian function. Because the quasielastic component of a QENS spectrum arises solely from incoherent scattering with the water molecules, the data across the entire Q range represent a direct probe of the water dynamics. The half-width at half-maximum (HWHM, Γ) of the best-fit Lorentzian at $\lambda = 2$, 6, and 16 as a function of

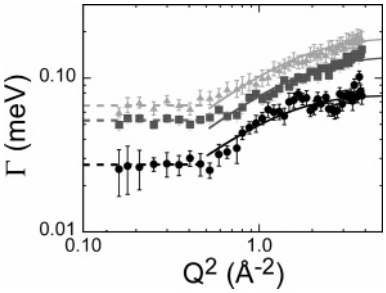

Figure 6. Half-width at half-maximum of the Lorentzian component of the QENS data plotted as a function of Q^2 for $\lambda = 2$ (●), 6 (■), and 16 (▲). The solid lines represent the best fit of the unbounded jump diffusion model to the data at $Q > 0.7$ Å^{-1}, and the dashed lines are the constant value y-intercepts of Γ at $Q < 0.7$ Å^{-1}.

Q^2 are given as data points in Figure 6. As expected, increasing the hydration level results in an overall increase in Γ because the dynamic behavior of water in the pores becomes more bulklike and less hindered by interactions with the hydrophilic domain. At all hydration levels, the Q dependent behavior of Γ follows a similar trend of constant value at low Q followed by increase in value at high Q.

Our interpretation of the quasielastic scattering from the hydrated PFSI membrane follows the procedures used in prior QENS investigations on water dynamics in porous glass,[45] zeolites,[46] and hydrogels.[47,48] Each of these studies, as here, indicates two distinct regimes of dynamical behavior with transition at wavevector Q^* between a constant Γ value at $Q < Q^*$ and increasing asymptotic dependence at $Q > Q^*$. As apparent from Figure 6, Q^* on the PFSI membrane at $\lambda = 2$, 6, and 16 is unchanged at approximately 0.7 Å^{-1} ($Q^2 \approx 0.5$ Å^{-2}). The flat, low Q regime is indicative of spatially confined diffusional behavior, whereas the Lorentzian line shapes at $Q > Q^*$ are characteristic of jump diffusion within the confining region. By using this combination of models to evaluate the dynamic behavior at different length scales, it is possible to account for both bounded continuous diffusion and atomic granularity, features not contained in any current single theoretical model.

By interpreting the QENS data with the continuous diffusion in a sphere model of Volino and Dianoux[30] at low Q and the unbounded jump diffusion model of Hall and Ross[37] at high Q, we were able to quantify the water dynamics within the hydrated PFSI membrane by extracting residence times and self-diffusion coefficients over each Q regime separately. The ability of this two-pronged approach to adequately describe the experimental data is illustrated by the dashed and solid lines of Figure 6, representing the best fits of the constant low Q value of Γ and the jump diffusion model at $Q > Q^*$, respectively. A complete list of the final results of our analysis, detailed below, is assembled in Table 2.

At low Q values, the diffusion in a sphere model predicts an asymptotic value of Γ. Consequently, the residence time of the local confinement is determined from $\Gamma_{Q\to 0} = 1/\tau_0$. Jump diffusion predicts an asymptotic limit as Q values become large. This asymptotic value has been determined by fitting the Q^2 data greater than 0.5 Å^{-2} with eq 7 using the Monte Carlo fitting procedure. The value of $\Gamma_{Q\to\infty}$ using the jump diffusion model is inversely proportional to the residence time between successive jumps of a single scattering site (τ_1). The characteristic confinement and jump residence times of water molecules within the PFSI membrane over all hydration levels are plotted in Figure 7. Both residence time parameters decrease as the membrane hydration increases, indicating an increased mobility of the water molecules as the hydrophilic domain grows.

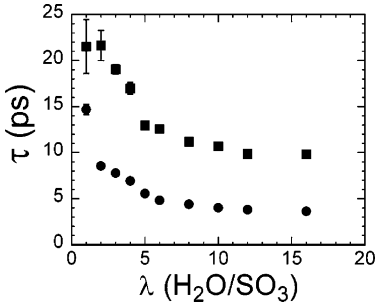

Figure 7. Plot of water molecule residence time (τ) in a perfluorosulfonated ionomer membrane based on unbounded jump diffusion at $Q > 0.7$ A^{-1} (●, τ_1) and diffusion confined within a sphere observed at $Q < 0.7$ A^{-1} (■, τ_0) as a function of membrane swelling. τ_1 corresponds to the time between successive jump motions and τ_0 is the characteristic time scale of interaction with the confining surface.

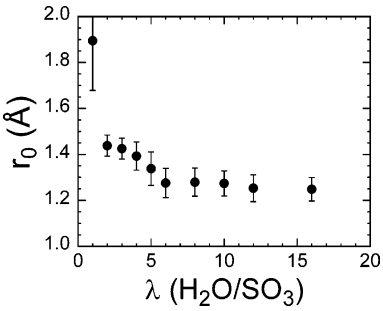

Figure 8. Mean jump length (r_0) obtained from the best fit of the half-width at half-maximum of the Lorentzian component at $Q > 0.7$ A^{-1} for random jump diffusion with a Gaussian distribution (eq 8) as a function of hydration.

TABLE 2: Values of the Self-Diffusion Coefficient and Mean Residence Time Obtained by Fitting the Half-Width at Half-Maximum of the Lorentzian Component of the QENS Data with the Confined Spherical Diffusion Model (D_{local}, τ_0) at $Q < 0.7$ Å^{-1} and the Unbounded Jump Diffusion Model (D_{jump}, τ_1) at $Q > 0.7$ Å^{-1}

λ	D_{local} (10^{-5} cm^2/s)	D_{jump} (10^{-5} cm^2/s)	τ_0 (ps)	τ_1 (ps)
1	0.38 ± 0.36	1.22 ± 0.08	27.0 ± 15.9	14.7 ± 1.1
2	0.46 ± 0.12	1.21 ± 0.03	22.3 ± 4.0	8.6 ± 0.3
3	0.53 ± 0.06	1.31 ± 0.03	19.1 ± 1.4	7.8 ± 0.3
4	0.60 ± 0.08	1.40 ± 0.05	17.1 ± 1.6	6.9 ± 0.3
5	0.79 ± 0.11	1.61 ± 0.07	13.0 ± 1.3	5.6 ± 0.4
6	0.81 ± 0.05	1.69 ± 0.07	12.5 ± 0.6	4.8 ± 0.4
8	0.91 ± 0.06	1.86 ± 0.08	11.2 ± 0.5	4.4 ± 0.3
10	0.95 ± 0.04	2.02 ± 0.07	10.7 ± 0.3	4.0 ± 0.2
12	1.03 ± 0.07	2.07 ± 0.08	9.8 ± 0.5	3.8 ± 0.2
16	1.04 ± 0.12	2.14 ± 0.08	9.8 ± 0.7	3.6 ± 0.3

Increased water mobility is further reflected in the jump length distance extracted from fits of the jump diffusion motion at $Q > Q^*$. From the model, the average jump length distance (r_0) is calculated from the fit of the Γ (eq 7) and the relation $\langle r^2 \rangle = 3r_0^2$. The value of r_0, plotted as a function of hydration, is given in Figure 8. The mean jump length displays a decreasing trend as the number of waters within the membrane increases to $\lambda \approx 6$, after which it remains relatively constant at around 1.25 Å. The observed hydration dependence of the jump length reflects a higher density of energetically favorable hydrogen orientations within the water clusters. As water is initially added to the system, the magnitude of unfavorable interactions between the water and the hydrophobic polymeric backbone diminishes because a greater number of water molecules are able to participate in favorable hydrogen bonding interactions with

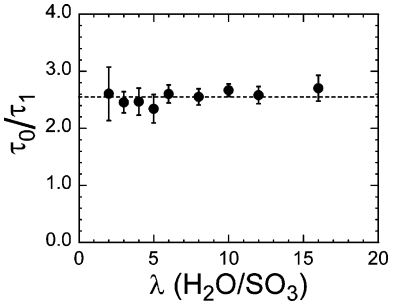

Figure 9. Plot of the frequency ratio of jump motions to interactions with the confining environment between $\lambda = 2$ and 16. The dotted line represents the average value over all hydration levels (2.55 ± 0.21).

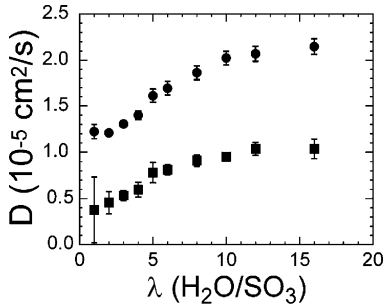

Figure 10. Self-diffusion coefficient of water in a perfluorosulfonated ionomer membrane as a function of hydration level calculated using the unbounded jump diffusion (●, D_{jump}) and confined diffusion in a sphere (■, D_{local}) models. The values were obtained by fitting the Q dependence of Γ at $Q > 0.7$ Å^{-1} at $Q < 0.7$ Å^{-1}, respectively.

various molecular orientations. The decreasing jump length is a reflection of the evolution of a more homogeneous energetic environment from the coarse-grain energetics present at low hydration levels. However, as the number of waters per sulfonate functionality increases beyond 6, the mean jump length remains constant, indicating that the hydrogen bonding reorientational freedom has reached near bulklike behavior. These results are in good agreement with the insight provided from isopiestic data on swelled PFSI membranes[49] and protonic defect models in bulk water.[50,51]

Separately analyzing the residence times on different length scales allows us to compare the frequency with which a jump motion occurs and how often the particles interact with the confining surface. Interestingly the ratio of τ_0/τ_1, representative of the average number of jump motions per surface interaction, is nearly constant over the entire swelling range. The values of τ_0/τ_1 are plotted in Figure 9 along with a dashed line representing the average value of 2.55 (error less than 10%). The fundamental feature of the PFSI membrane reflected by τ_0/τ_1 may prove insightful for understanding relative rates of proton hopping to proton vehicular transport in a PFSI membrane and how the contributions from each affects overall conductivity across a functioning membrane.

At low Q, the confined spherical diffusion model predicts a constant value of the quasielastic broadening through the relationship $\Gamma_{Q\to 0} = 4.33\, D_{local}/R^2$, where D_{local} is the diffusion coefficient of confinement and R is the radius of the characteristic confinement volume obtained from analysis of the EISF. At $Q > Q^*$, the unconstrained jump diffusion model predicts a diffusion coefficient (D_{jump}) from the values of $\langle r^2 \rangle$ and τ_1 using the relation given in eq 8. The values of the diffusion coefficients predicted by both models from the quasielastic broadening at all hydration levels are given in Figure 10. As the hydrophilic domain of the membrane swells with water, the diffusion coefficients obtained from each model display similar trends: increasing in value toward an asymptotic maximum.

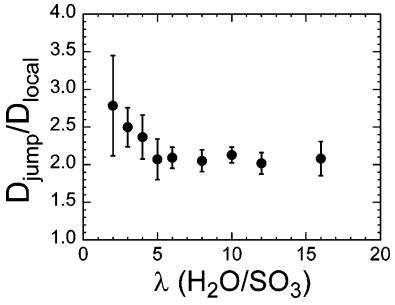

Figure 11. Plot of the relative diffusion coefficient ratios extracted from the quasielastic data at all hydration levels based on the jump diffusion model at $Q > 0.7$ Å^{-1} and confined diffusion within a sphere model at $Q < 0.7$ Å^{-1}.

When swelled to high hydration levels, the diffusion coefficients tend toward asymptotic values of approximately 1.1×10^{-5} and 2.2×10^{-5} (cm^2/s) for spherical and jump diffusion models, respectively. The value of D_{jump} as the membrane nears saturation is slightly less than the 2.36×10^{-5} cm^2/s value obtained from neutron scattering measurement of bulk water diffusion at 292 K[52] and identical to the value obtained from water diffusion in an agarose gel at 294 K.[53] D_{local} near saturation, however, is less than half of that of bulk water. Again, this difference is reflective of the spherical diffusion model being more sensitive to the longer length-scale motions associated with interaction between the water molecules and the polymer matrix. Additionally, it is not surprising that the values of the diffusion coefficient obtained here are greater than those obtained using the NMR technique[22] because NMR probes diffusive behavior on the millisecond (rather than picosecond) time scale and is more sensitive to the hindered motions between the water and polymer that occur on a microscopic scale.[25,29]

Although D_{jump} and D_{local} have similar trends with increasing water content, the relative value of the two diffusion coefficients displays interesting behavior. A plot of this ratio (D_{jump}/D_{local}) is illustrated in Figure 11. Over the swelling regime of $\lambda > 5$, the relative values of D_{jump} and D_{local} remain nearly constant at a ratio of approximately 2. With decreasing water content, however, the D_{local} decreases more rapidly than D_{jump} corresponding to the increased value in the ratio of D_{jump}/D_{local} at low hydration. An intriguing similarity between this behavior and that of the relative ratio of ionic conductivity to water diffusion coefficient[24] may prove insightful for rationalizing the protonic conductivity based on jump motions of the water molecules.

Conclusions

The dynamic behavior of water molecules within a swelled PFSI membrane has been measured with QENS, and the data have been interpreted on the basis of confined diffusion in a sphere and unconstrained random jump diffusion models. The dynamic radius of spherical confinement and fraction of nondiffusing hydrogen atoms obtained by fitting the EISF to the theoretical continuous diffusion in a sphere model reflect preferential swelling within the hydrophilic domain of the PFSI and a single nondiffusing hydronium ion over the picosecond time window of the QENS experiment. Quantitative analysis of the diffusive behavior of the water molecules was performed by separately analyzing the quasielastic neutron scattering below and above $Q = 0.7$ Å^{-1}. All of the extracted parameters follow a similar behavior that changes rapidly over low swelling

conditions, tending toward asymptotic values. Overall, the observed dynamic behavior reflects the general distribution of water molecules within the hydrophilic phase of the PFSI: initial hydration results in water molecules forming a close hydration shell proximate to the sulfonic acid functionality of the PFSI that becomes more loosely bound as the hydration increases, ultimately tending toward bulklike behavior.

The results of this study expand current understanding of the interplay between physical and chemical properties of PFSI membranes and the dynamic behavior of water molecules when the PEM is hydrated. By changing the swelling condition of the membrane from dry to near saturation, it was possible to mimic the actual operating conditions that a PEFC will be required to endure and ascertain the water dynamics that are critical to effective fuel cell performance. It is hoped that these results will promote the advancement of PEFCs by providing a measurement technique able to measure water dynamics under a wide range of conditions that ultimately will enable directed design of polymeric materials able to achieve optimal protonic conduction under the target range of operating conditions.

Acknowledgment. We thank Dan A. Neumann, Robert M. Dimeo, and Ronald L. Cappelletti of the NIST Center for Neutron Research for assistance in the preparation of this manuscript. We also acknowledge the support of the National Institute of Standards and Technology, U.S. Department of Commerce, in providing the neutron research facilities used in this work.

References and Notes

(1) Brandon, N. P.; Skinner, S.; Steele, B. C. H. *Annu. Rev. Mater. Res.* **2003**, *33*, 183.
(2) Steele, B. C. H.; Heinzel, A. *Nature* **2001**, *414*, 345.
(3) Zawodzinski, T. A.; Derouin, C.; Radzinski, S.; Sherman, R. J.; Smith, V. T.; Springer, T. E.; Gottesfeld, S. *J. Electrochem. Soc.* **1993**, *140*, 1041.
(4) Paddison, S. J. *Annu. Rev. Mater. Res.* **2003**, *33*, 289.
(5) Giotto, M. V.; Zhang, J.; Inglefield, P. T.; Wen, W.-Y.; Jones, A. A. *Macromolecules* **2003**, *36*, 4397.
(6) Meresi, G.; Wang, Y.; Bandis, A.; Inglefield, P. T.; Jones, A. A.; Wen, W.-Y *Polymer* **2001**, *42*, 6153.
(7) Young, S. K.; Trevino, S. F.; Beck Tan, N. C. *J. Polym. Sci. Part B: Polym. Phys.* **2002**, *40*, 387.
(8) Rollet, A.-L.; Diat, O.; Gebel, G. *J. Phys. Chem. B* **2002**, *106*, 3033.
(9) Rollet, A.-L.; Gebel, G.; Simonin, J.-P.; Turq, P. *J. Polym. Sci. Part B: Polym. Phys.* **2001**, *39*, 548.
(10) Haubold, H.-G.; Vad T.; Jungbluth, H.; Hiller, P. *Electrochim. Acta* **2001**, *46*, 1559.
(11) Gebel, G. *Polymer* **2000**, *41*, 5829.
(12) Gebel, G.; Moore, R. B. *Macromolecules* **2000**, *33*, 4850.
(13) Gebel, G.; Lambard, J. *Macromolecules* **1997**, *30*, 7914.
(14) Gruger, A.; Régis, A.; Schmatko, T.; Colomban, P. *Vibr. Spectrosc.* **2001**, *26*, 215.
(15) Ludvigsson, M.; Lindgren, J.; Tegenfeldt, J. *Electrochim. Acta* **2000**, *45*, 2267.
(16) Wang, Y.; Kawano, Y.; Aubuchon, S. R.; Palmer, R. A. *Macromolecules* **2003**, *36*, 1138.
(17) Liang, Z.; Chen, W.; Liu, J.; Wang, S.; Zhou, Z.; Li, W.; Sun, G.; Xin, Q. *J. Membr. Sci.* **2004**, *233*, 39.
(18) James, P. J.; McMaster, T. J.; Newton, J. M.; Miles, M. J. *Polymer* **2000**, *41*, 4223.
(19) James, P. J.; Elliott, J. A.; McMaster, T. J.; Newton, J. M.; Elliott, A. M. S.; Hanna, S.; Miles, M. J. *J. Mater. Sci.* **2000**, *35*, 5111.
(20) Jang, S. S.; Molinero, V.; Çağin, T.; Goddard, W. A., III. *J. Phys. Chem. B* **2004**, *108*, 3149.
(21) Vishnyakov, A.; Neimark, A. V. *J. Phys. Chem. B* **2001**, *105*, 9586.
(22) Zawodzinski, T. A.; Neeman, M.; Sillerud, L. O.; Gottesfeld, S. *J. Phys. Chem.* **1991**, *95*, 6040.
(23) Kreuer, K.-D. *J. Membr. Sci.* **2001**, *185*, 29.
(24) Kreuer, K. D. *Solid State Ionics* **1997**, *97*, 1−15.
(25) Kreuer, K.-D.; Dippel, T.; Meyer, W.; Maier, J. *Mater. Res. Soc. Symp. Proc.* **1993**, *293*, 273.
(26) Zawodzinski, T. A.; Neeman, M.; Sillerud, L. O.; Gottesfeld, S. *J. Phys. Chem.* **1991**, *95*, 6040.
(27) Gong, X.; Bandis, A.; Tao, A.; Meresi, G.; Wang, Y.; Inglefield, P. T.; Jones, A. A.; Wen, W.-Y. *Polymer* **2001**, *42*, 6485.
(28) Jayakody, J. R. P.; Stallworth, P. E.; Mananga, E. S.; Farrington-Zapata, J.; Greenbaum, S. G. *J. Phys. Chem. B* **2004**, *108*, 4260.
(29) Rollet, A.-L.; Simonin, J.-P.; Turq, P.; Gebel, G.; Kahn, R.; Vandais, A.; Noel, J.-P.; Malveau, C.; Canet, D. *J. Phys. Chem. B* **2001**, *105*, 4503.
(30) Volino, F.; Dianoux, A. J. *Mol. Phys.* **1980**, *41*, 271.
(31) Volino, F.; Pineri, M.; Dianoux, A. J.; De Geyer, A. *J. Polym. Sci. Polym. Phys.* **1982**, *20*, 481.
(32) A complete atomic listing of neutron scattering lengths and cross sections can be found at http://www.ncnr.nist.gov/resources/n-lengths/.
(33) Detailed information on the NG6 FCS instrument can be found on the NCNR website at www.ncnr.nist.gov/instruments/fcs/.
(34) Doster, W.; Diehl, M.; Gebhardt, R.; Lechner, R. E.; Pieper, J. *Chem. Phys.* **2003**, *292*, 487.
(35) For more information regarding the xtreat data analysis program, see http://www.ncnr.nist.gov/staff/craig/.
(36) Beé, M. *Quasi-elastic neutron scattering: principles and application in solid-state chemistry, biology, and materials science*; Hilger, A., Ed.; Bristol: Philadelphia, 1988.
(37) Hall, P. L.; Ross, D. K. *Mol. Phys.* **1981**, *42*, 673.
(38) Press, W. H.; Flannery, B. P.; Teukolsky, S. A.; Vetterling, W. T. *Numerical Recipes, The Art of Scientific Computing;* Cambridge University Press: Cambridge, U.K., 1986.
(39) Carlsson, P.; Zorn, R.; Andersson, D.; Farago, B.; Howells, W. S.; Borjesson, L. *J. Chem. Phys.* **2001**, *114*, 9645.
(40) Beé, M. *Physica B* **1992**, *182*, 323.
(41) Iwamoto, R.; Oguro, K.; Sato, M.; Iseki, Y. *J. Phys. Chem. B* **2002**, *106*, 6973.
(42) Gruger, A.; Régis, A.; Schmatko, T.; Colomban, P. *Vibr. Spectrosc.* **2001**, *26*, 215.
(43) Buzzoni, R.; Bordiga, S.; Ricchiardi, G.; Spoto, G.; Zecchina, A. *J. Phys. Chem.* **1995**, *99*, 11937.
(44) Li, T.; Wlaschin, A. Balbuena, P. B. *Ind. Eng. Chem. Res.* **2001**, *40*, 4789.
(45) Bellissent-Funel, M.-C.; Chen, S. H.; Zanotti, J.-M. *Phys. Rev. E* **1995**, *51*, 4558.
(46) Crupi, V.; Majolino, D.; Migliardo, P.; Venuti, V.; Wanderlingh, U.; Mizota, T.; Telling, M. *J. Phys. Chem. B* **2004**, *108*, 4314.
(47) Paradossi, G.; Cavalieri, F.; Chiessi, E.; Telling, M. T. F. *J. Phys. Chem. B* **2003**, *107*, 8363.
(48) Paradossi, G.; Di Bari, M. T.; Telling, M. T. F.; Turtu, A.; Cavalieri, F. *Physica B* **2001**, *301*, 150.
(49) Zawodzinski, T. A.; Springer, T. E.; Davey, J.; Jestel, R.; Lopez, C.; Valerio, J.; Gottesfeld, S. *J. Electrochem. Soc.* **1993**, *140*, 1981.
(50) Kornyshev, A. A.; Kuznetsov, A. M.; Spohr, E.; Ulstrup, J. *J. Phys. Chem B* **2003**, *107*, 3351.
(51) Kreuer, K. D. *Solid State Ionics* **2000**, *136−137*, 149.
(52) Cavatorta, F.; Deriu, A.; Di Cola, D.; Middendorf, H. D. *J. Phys.: Condens. Matter* **1994**, *6*, A113.
(53) Middendorf, H. D.; Di Cola, D.; Cavatora, F.; Deriu, A.; Carlile, C. J. *Biophys. Chem.* **1994**, *53*, 145.